

Jets and Photons in ALICE

Thomas Dietel for the ALICE Collaboration

*Westfälische-Wilhelms-Universität Münster
Wilhelm-Klemm-Str 9
48149 Münster
Germany*

Abstract.

ALICE measured transverse momentum spectra of π^0 and η mesons via the two photon decay in pp collisions at $\sqrt{s} = 0.9, 2.76$ and 7 TeV and Pb-Pb collisions at $\sqrt{s_{NN}} = 2.76$ TeV. NLO pQCD calculations agree with pp measurements at 0.9 TeV, but overestimate the data at 2.76 and 7 TeV. The nuclear modification factor for neutral pions shows a strong suppression of high- p_T particle production in central Pb-Pb collisions.

Raw spectra of charged particle jets have been measured in Pb-Pb collisions. Detailed studies of background fluctuations have been performed and will allow us to unfold the spectra even for low momentum cut offs, giving access to soft fragmentation products in quenched jets.

Keywords: ALICE, LHC, heavy-ion collisions, quark-gluon plasma, hard scattering, jet quenching, nuclear modification factor

PACS: 13.85.-t, 25.70.Bh, 25.70.Cj, 25.75.Dw

INTRODUCTION

The interaction of high-momentum partons with hot and dense nuclear matter is a key point to the understanding of heavy-ion collisions. The energy loss of these partons during the traversal of the medium is called jet quenching [1]. It results in a suppression of particle production at high transverse momenta, as measured with the nuclear modification factor R_{AA} for hadrons [2]. A second consequence is the increased production of soft particles associated with the original high-momentum parton to ensure energy and momentum conservation. This low- p_T enhancement is observable in the modification of fragmentation functions derived from fully reconstructed jets [3].

ALICE DETECTOR AND DATA SETS

The ALICE detector at the CERN LHC was designed for the study of the quark-gluon plasma created in high-multiplicity heavy-ion collisions. The central barrel with a large Time Projection Chamber (TPC) and the Inner Tracking System (ITS) with 6 layers of silicon detectors provides tracking with full azimuthal acceptance in $|\eta| < 0.9$. ALICE also features two electromagnetic calorimeters at mid-rapidity: the fine-granularity PHOS covering $|\eta| < 0.13$ and $\Delta\phi = 60^\circ$ and the EMCal with coarser granularity but larger acceptance of $|\eta| < 0.7$ and $\Delta\phi = 40^\circ$ in 2010, increased to $\Delta\phi = 100^\circ$ in 2011.

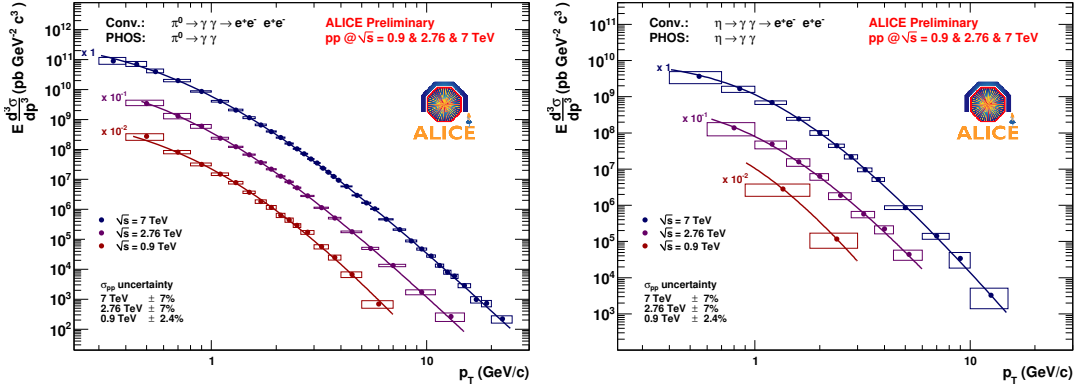


FIGURE 1. Invariant cross sections for π^0 (left) and η (right) mesons in pp collisions at $\sqrt{s} = 0.9, 2.76$ and 7 TeV. The data points represent the weighted average of conversion and PHOS measurements and were parameterized with a Tsallis function $Ed^3\sigma/dp^3 \propto (1 + (m_T - m)/(nT))^{-n}$

The data presented here are from pp runs at $\sqrt{s} = 0.9$ and 7 TeV taken in 2010, the first Pb-Pb run at $\sqrt{s_{NN}} = 2.76$ TeV in fall 2010 and a pp run at the reference energy of $\sqrt{s} = 2.76$ TeV in spring 2011.

NEUTRAL MESON PRODUCTION IN PP COLLISIONS

p_T spectra of neutral mesons in pp collisions are not only an important reference for Pb-Pb collisions, but also test perturbative QCD at the highest available energies. With calculable parton cross-sections and parton distribution functions in the relevant kinematic region well under control, the main uncertainty comes from fragmentation functions. Pion production with $p_T < 20$ GeV/c at top LHC energy is dominated by gluon fragmentation, but the gluon fragmentation functions are poorly constrained by measurements of pp collisions at lower energies and e^+e^- collisions. Neutral meson spectra at LHC energies therefore provide important constraints on gluon fragmentation functions.

ALICE has measured neutral pions and η mesons in pp collisions at $\sqrt{s} = 0.9, 2.76$ and 7 TeV using the invariant mass of their two-photon decays, where the photons were either detected by the PHOS or via conversions with the TPC and ITS [4].

Figure 1 shows the combined invariant cross sections for $p + p \rightarrow \pi^0 + X$ (left) and $p + p \rightarrow \eta + X$ (right) obtained from the conversion and the PHOS measurements of neutral pions and eta mesons. The data are fully corrected, including a small correction (up to 20%) to account for the variation within one bin. The spectra are fitted with a Tsallis function to facilitate comparisons between the two reconstruction methods and with NLO calculations.

Figure 2 compares the conversion and PHOS methods to measure the invariant cross section. Shown is the ratio of both methods to the Tsallis parameterisation of the combined spectra from Figure 1. Both measurements agree very well within their error bars.

The π^0 cross section is compared to an NLO pQCD calculation using the CTEQ6M5

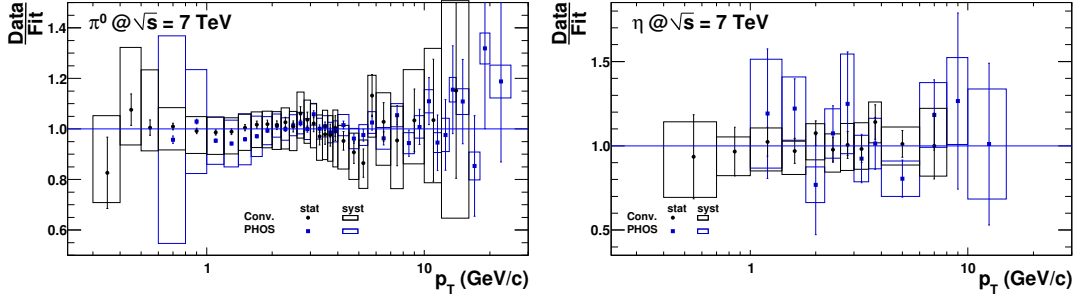


FIGURE 2. Ratio of p_T spectra measured with conversions (black) and PHOS (black) to the Tsallis parameterisation for π^0 (left) and η (right) mesons in pp collisions at $\sqrt{s} = 7$ TeV.

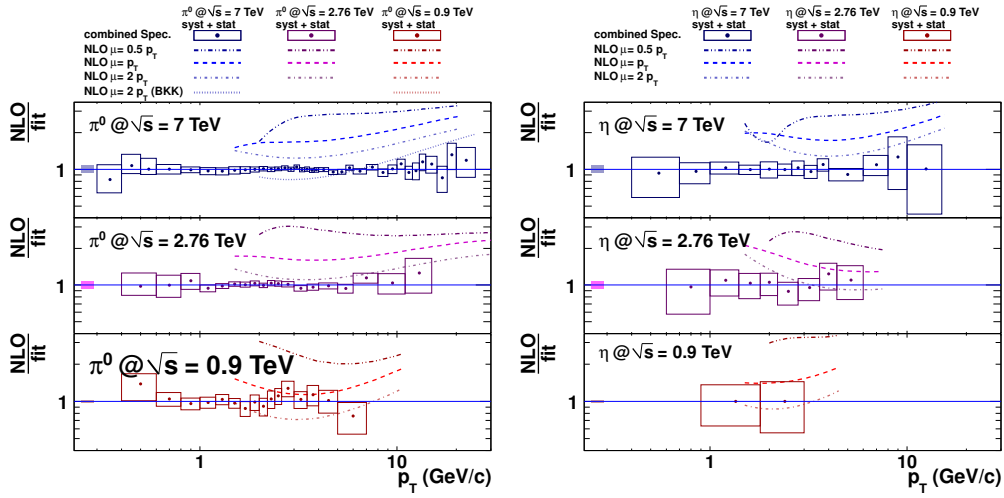


FIGURE 3. Comparison of data and NLO pQCD calculations, normalized to the Tsallis fit from Figure 1. For details about the calculations see text.

parton distribution functions [5] and DSS fragmentation functions [6]. The theoretical uncertainty of the calculation has been estimated by varying unphysical scales $\mu = 0.5p_T, p_T, 2p_T$ [7]. Figure 3 shows the NLO calculation, normalized to the Tsallis fit, in comparison with the measured spectra. For $\sqrt{s} = 0.9$ TeV, the calculation agrees with the data, while for higher energies it overestimates the data. At 7 TeV a second calculation [8] using the BKK FF [9] shows better agreement with the data. The left panel in Figure 3 compares the measured η spectra with an NLO calculation using the AESSS FF [10]. The trend is similar to the DSS FF in pion data, showing agreement at 0.9 TeV and an overestimation at higher energies of 2.76 and 7 TeV.

NUCLEAR MODIFICATION FACTOR FOR PIONS

The modification of spectra in heavy-ion collisions is commonly expressed with the nuclear modification factor R_{AA} , defined as the ratio of production rates in nucleus-nucleus and pp collisions, scaled by the number of binary nucleon-nucleon interactions

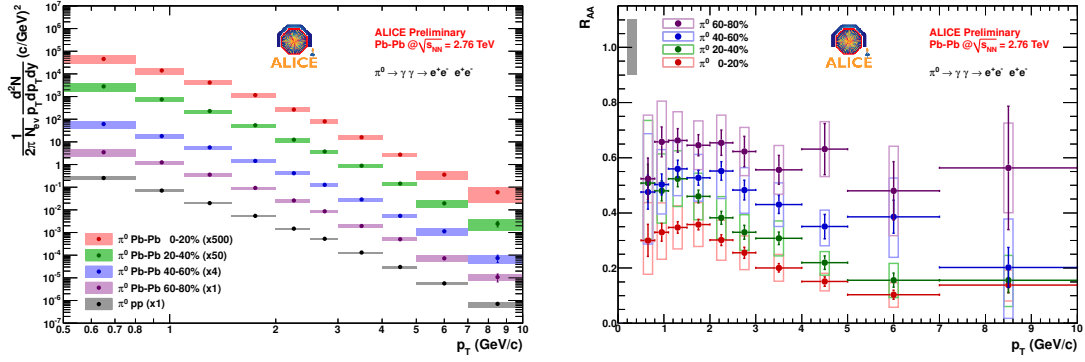


FIGURE 4. π^0 yield (left) and nuclear modification factor R_{AA} (right) in Pb-Pb collisions at $\sqrt{s_{NN}} = 2.76$ TeV in 4 centrality bins. The left panel also shows the π^0 yield in pp collisions.

as determined from a Glauber calculation:

$$R_{AA} = \frac{1}{\langle N_{coll} \rangle} \frac{(1/N_{evt}^{AA}) d^2 N_{\pi^0}^{AA} / dy dp_T}{(1/N_{evt}^{pp}) d^2 N_{\pi^0}^{pp} / dy dp_T}$$

The yield of neutral pions in Pb-Pb collisions at $\sqrt{s_{NN}} = 2.76$ TeV taken in fall 2010 has been measured by ALICE using the conversion method [11]. The yields as a function of p_T for 4 different centrality bins are shown in the left panel of Figure 4, together with the yield for pp collisions. The right panel shows the nuclear modification factor R_{AA} for the same 4 centrality bins. A clear suppression of high- p_T hadron production can be seen that increases from peripheral to central collisions. The maximum suppression is reached at $p_T \approx 6$ GeV/c with an $R_{AA} \approx 0.1$, consistent with the suppression of charged hadrons [12]. The observed suppression is stronger than at RHIC, where PHENIX reported a value of 0.2 to 0.3 [13].

JET RECONSTRUCTION AND BACKGROUND FLUCTUATIONS

Full jet reconstruction can provide a complementary picture to the suppression of single particles as discussed in the previous section. By accounting for low- p_T particles, the energy lost due to jet quenching can be recovered, so that the redistribution of energy and momentum in the quenching process can be studied in terms of medium-modified fragmentation functions. In order to be sensitive to jet modifications it is extremely important to minimize the bias on hard fragmentation by applying the lowest possible momentum cut off during jet reconstruction.

We applied various cone and sequential recombination jet reconstruction algorithms to Pb-Pb collisions. Lacking large acceptance calorimetry in 2010, the algorithms from the FastJet package were run on charged tracks only with a radius/distance parameter of 0.4. For this study, we use the anti- k_T jet finder and subtract the background density ρ as determined by calculating the median p_T /area of reconstructed k_T clusters [14].

Figure 5 shows raw jet spectra for different centralities, reconstructed with a track momentum cut off of $p_T > 150$ MeV/c (left) and $p_T > 2$ GeV/c (right). While the shapes

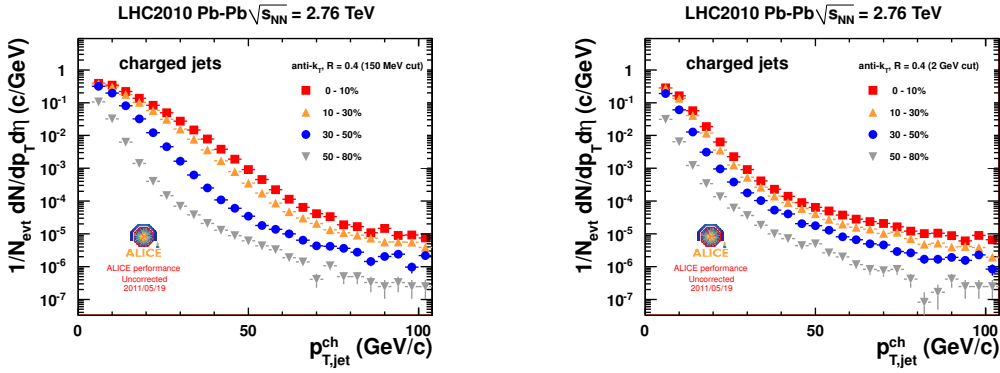


FIGURE 5. Raw jet spectra for different centralities using the anti- k_T jet finder on charged tracks, after background subtraction. In the left panel, a track cut of $p_T > 150 \text{ MeV}/c$ was used, in the right panel $p_T > 2 \text{ GeV}/c$.

in the peripheral and central event classes are similar for the high threshold, a strong modification is visible for the low threshold. This difference is caused by background fluctuations in central events that predominantly appear at low transverse momenta.

These background fluctuations can be studied using different probes in Pb-Pb collisions: random cones ($R=0.4$), where the p_T of all tracks in the cone is summed, embedded single high- p_T tracks and embedded PYTHIA-jets. In case of embedding, the same anti- k_T jet finder as for unmodified events is run and the reconstructed jets are matched to the embedded probe by finding the track or 50% of the embedded jet momentum. We then define the residuals of the jet measurements as

$$\delta p_T = p_T^{rec} - A \cdot \rho - p_T^{probe}$$

where $p_T^{probe} = 0$ for random cones. The residuals for random cones are also analyzed for events where all tracks were randomized in η and ϕ and where the leading two jets in each event were excluded.

The residuals for random cones, shown in the left panel of Figure 6, exhibit an assymmetric shape that follows a Gaussian distribution for $\delta p_T < 0$ and has a tail towards high p_T . This tail can be attributed to the onset of jet production, which is confirmed when the leading two jets are excluded: the distribution becomes Gaussian and is only sensitive to background fluctuations. For randomized events, we again see a Gaussian distribution, but with a smaller width than before. This indicates that the randomization did not only destroy jet-like correlations, but also other region-to-region fluctuations like e.g. elliptic flow.

The right panel in Figure 6 compares the random cones with embedded tracks and jets. The residuals obtained for these probes are consistent with each other and also match the scaled raw jet spectrum. This confirms that the broadening of the jet spectrum for the low momentum cut off is caused by background fluctuations. Unfolding of the jet spectra will therefore be necessary. The fact that the mean of the Gaussian distributions, as determined from fits to the left hand side, is close to 0 affirms the validity of the background subtraction.

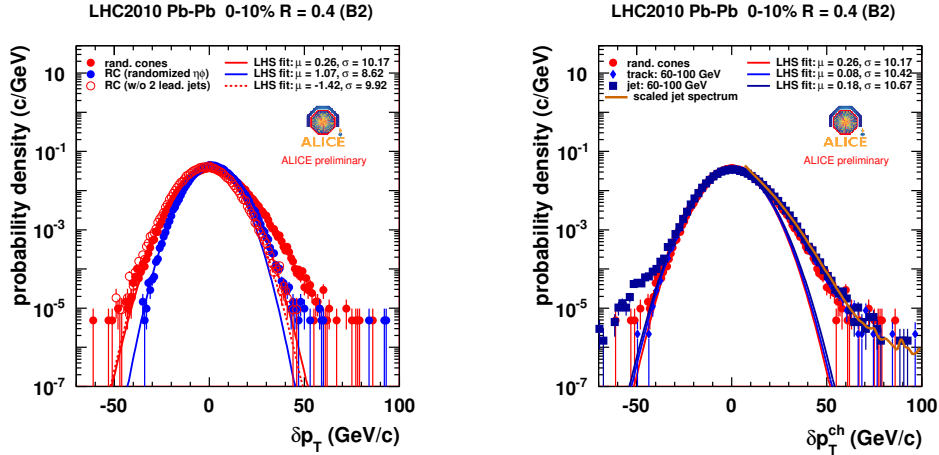


FIGURE 6. Left panel: difference of embedded and reconstructed energy (residuals) for random cones in unmodified and randomized events, and events with the two leading anti- k_T cluster excluded. Right panel: residuals for random cones, embedded tracks and embedded jets, compared to the scaled raw jet spectrum.

CONCLUSIONS

π^0 and η invariant cross sections were measured in pp collisions at $\sqrt{s} = 0.9, 2.76$ and 7 TeV. None of the considered NLO pQCD calculations can reproduce the data at all available energies.

The nuclear modification factor for π^0 production was determined from pp and Pb-Pb collisions at $\sqrt{s_{NN}} = 2.76$ TeV. A stronger suppression of high- p_T particles than at RHIC energies was found, consistent with charged particle measurements of ALICE.

Jet reconstruction even in the most central Pb-Pb collisions is possible, but subject to large background fluctuations. These fluctuations were studied by placing random cones and embedded tracks and jets in real events.

REFERENCES

1. J. D. Bjorken, FERMILAB-Pub-82/59-THY (1982),.
2. C. Adler *et al.*, *Phys. Rev. Lett.* **89**, 202301 (2002).
3. C. A. Salgado, and U. A. Wiedemann, *Nucl. Phys.* **A715**, 783–786 (2003).
4. K. Reygers, *to appear in J.Phys.G* (2011), arXiv:1106.5932.
5. J. Pumplin, D. R. Stump, J. Huston, H.-L. Lai, P. Nadolsky, and W.-K. Tung, *JHEP* **2002**, 012 (2002).
6. D. de Florian, R. Sassot, and M. Stratmann, *Phys. Rev. D* **75**, 1–26 (2007).
7. B. Jäger, A. Schäfer, M. Stratmann, and W. Vogelsang, *Phys. Rev. D* **67**, 1–10 (2003).
8. P. Aurenche, M. Fontannaz, J. P. Guillet, B. A. Kniehl, and M. Werlen, *Eur.Phys.J.* **C13**, 347 (1999).
9. J. Binnewies, B. a. Kniehl, and G. Kramer, *Z. Phys. C* **65**, 471 (1995).
10. C. Aidala, F. Ellinghaus, R. Sassot, J. Seele, and M. Stratmann, *Phys. Rev. D* **83**, 1–11 (2011).
11. G. Conesa Balbastre, *to appear in J.Phys.G* (2011).
12. K. Aamodt *et al.* *Phys. Lett. B* **696**, 30–39 (2011).
13. S. Adler *et al.* *Phys. Rev. Lett.* **91**, 1–6 (2003).
14. C. Klein-Boesing, *to appear in J.Phys.G* (2011), arXiv:1106.4303.